MRN and Topoisomerase IIIα-RMI1/2 synchronize DNA resection motor proteins

Michael M. Soniat[1,2,*], Giaochau Nguyen[1,2], Hung-Che Kuo[1,2], Ilya J. Finkelstein[1,2,3,*]

[1] Department of Molecular Biosciences, The University of Texas at Austin, Austin, TX 78712 USA.
[2] Center for Systems and Synthetic Biology, The University of Texas at Austin, Austin, TX 78712 USA.
[3] Lead Contact
* Correspondence:
Michael M. Soniat: msoniat@utexas.edu
Ilya K Finkelstein: ilya@finkelsteinlab.org

Abstract

DNA resection—the nucleolytic processing of broken DNA ends—is the first step of homologous recombination. Resection is catalyzed by the resectosome, a multi-enzyme complex that includes BLM helicase, DNA2 or EXO1 nucleases, and additional DNA-binding proteins. Although the molecular players have been known for over a decade, how the individual proteins work together to regulate DNA resection remain unknown. Using single-molecule imaging, we characterized the roles of MRN and TOP3A-RMI1/2 during long-range DNA resection. BLM partners with TOP3A-RMI1/2 to form the BTRR complex (or BLM dissolvasome). TOP3A-RMI1/2 aids BLM in initiating DNA unwinding, and along with MRN, stimulates DNA2-mediated resection. Furthermore, MRN promotes the association between BTRR and DNA, and synchronizes BLM and DNA2 translocation to prevent BLM from pausing during resection. Together, this work provides direct observation of how MRN and DNA2 harness the BTRR complex to resect DNA efficiently and how TOP3A-RMI1/2 regulates BLM's helicase activity to promote efficient DNA repair.

Keywords: DNA resection, double-strand break, single-molecule, DNA curtains, BLM, DNA2

Introduction

Homologous recombination (HR) is one of two major eukaryotic double-strand DNA break (DSB) repair pathways. HR uses the intact sister chromatid during the S/G2 phase to promote error-free repair of DSBs (1, 2). HR initiates when the resection machinery, termed the resectosome, assembles to process (resect) the genome to generate kilobase-length stretches of single-stranded DNA (ssDNA) (3–12). The resectosome is a multi-enzyme complex composed of a helicase, a nuclease, and regulatory proteins. In humans, resection is initiated when MRE11-RAD50-NBS1 (MRN) and CtIP make an initial incision at the DSB (11, 13). This aids in the assembly of the core resectosome consisting of the Bloom Syndrome Helicase (BLM) along with Exonuclease 1 (EXO1) or DNA2 nuclease/helicase (**Figure 1A**) (7, 10). The resulting ssDNA produced by the resectosome is rapidly bound by the ssDNA-binding protein Replication Protein A (RPA), which protects the ssDNA from degradation before being replaced by the RAD51 recombinase for downstream homology search (14–17).

Accessory proteins regulate DNA resection to both initiate in a timely manner and to prevent over-resection and subsequent loss of genetic information (8, 12, 18). For example, in *S. cerevisiae*, the Sgs1 helicase (BLM homolog) and Dna2 nuclease/helicase interact with Mre11-Rad50-Xrs2 (MRX; the MRN homolog) and Top3-Rmi1 for efficient DNA resection (19, 20). The MRN complex has both exo- and endonuclease activity which is important for initial processing and the removal of protein adducts at DSBs (21–26). In addition to its nuclease-dependent roles, MRN/X also stimulates DNA resection via an incompletely understood nuclease-independent mechanism (19, 20, 27–32). The human homologs of the *S. cerevisiae* Top3-Rmi1 are TOP3A (a type 1A topoisomerase) and the heterodimer RMI1-RMI2 (yeast don't encode an RMI2 homolog). These proteins interact with BLM to form the BTRR complex (also known as the BLM dissolvasome) (33–39). BTRR participates in DNA resection, double Holliday junction dissolution, resolution of ultra-fine bridges, replication fork reversal, and interstrand crosslink repair (40–43). During the initial stages of HR, the

BTRR complex promotes long-range DNA2-mediated resection (44, 45). In later stages of HR, following RAD51 loading and strand invasion, BTRR is critical for the branch migration of Holliday junctions to form a hemicatenane, followed by decatenation by TOP3A-RMI1/2, resulting in non-crossovers (46, 47). Though the role of TOP3A-RMI1/2 is well defined in the later stages of HR, their precise roles in DNA resection remain unclear. For example, a catalytically inactive TOP3A mutant stimulates long-range DNA resection *in vitro*, suggesting that TOP3A-RMI1/2 may play a non-enzymatic role in resectosome assembly and/or translocation (20, 44).

Here, we use single-molecule fluorescence imaging to decipher the functions of individual resectosome components during DNA resection. MRN and TOP3A-RMI1/2 both help BLM to initiate DNA unwinding. MRN and TOP3A-RMI1/2 also stimulate DNA2-mediated resection. Finally, MRN synchronizes the translocation speeds of BLM and DNA2 to prevent BLM pausing. We reveal that MRN and TOP3A-RMI1/2 are regulatory resectosome components that initiate DNA resection and synchronize the individual motors during kilobase-long DNA processing.

Results

MRN and TOP3A-RMI1/2 together stimulate the DNA2 resectosome
To understand how MRN and TOP3A-RMI1/2 regulate DNA processing, we adapted our single-molecule resection assay to quantify the movement of DNA2 or EXO1 in complex with MRN and BLM-TOP3A-RMI1/2 (BTRR; **Figure 1**) (28, 48–50). We purified RMI1/2 with an N-terminal FLAG epitope on the RMI2 subunit. TOP3A-RMI1/2 was reconstituted by mixing TOP3A and RMI1/2 in a 1:3 ratio, followed by size exclusion chromatography. These three proteins formed a stable complex that eluted as a single peak on a Superose 6 column (**Figure S1**). TOP3A-RMI1/2 was then mixed with BLM to assemble the BTRR resectosome and labeled with fluorescent anti-FLAG antibodies (targeting RMI2 as described above). Biotinylated MRN was conjugated with streptavidin quantum dots (QDs) that emit in spectrally distinct
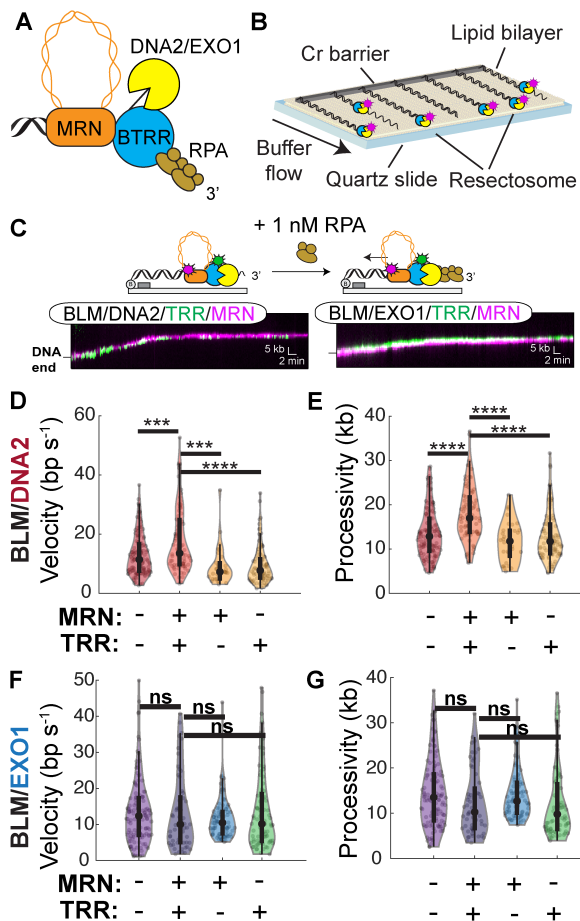
Figure 1. MRN and TOP3A-RMI1/2 stimulate DNA2-mediated resection. (A) Schematic of the human resectosome, consisting of MRE11-RAD50-NBS1 (MRN; orange), the nucleases DNA2 or EXO1 (yellow), BLM-TOP3A-RMI1/2 (blue), and Replication Protein A (RPA; brown). (B) Schematic of single-molecule resection assay (C) Representative kymograph of MRN (magenta), BTRR (green), and DNA2 or EXO1 resecting DNA. (D) Velocities and (E) processivities of BLM/DNA2 with and without TOP3A-RMI1/2 or MRN complex (N>50 for all experiments). Black bars show the interquartile range (thick bars) and 95% confidence intervals (thin bars). The black dot in the middle is the median. (F) Velocities and (G) processivities of BLM/EXO1 with and without TOP3A-RMI1/2 or MRN complex (N>50 for all experiments). (not significant; ns, p>0.05; ****, p<0.0001).

channels (**Figure S1**). We have previously confirmed that fluorescent MRN retains its biochemical activities (28). For the single-molecule resection assay, 48.5 kb-long double-stranded DNAs with biotin on one end and a 78 nt 3'-overhang on the opposite end are organized on the surface of a microfluidic flowcell (**Figure 1B**)(49, 51). Fluorescent BTRR complex is incubated with MRN and DNA2 or EXO1 before being injected into flowcells for single-molecule imaging. As expected, MRN and BTRR in complex with DNA2 and EXO1 bound the free DNA ends and resected the DNA in the presence of 1 nM RPA (**Figure 1C**). The MRN/BTRR/DNA2 complex resected DNA for 18 ± 6 kb (mean ± st. dev; n=82) with a velocity of 18 ± 11 bp s^{-1}. Omitting either TOP3A-RMI1/2 or MRN decreased BLM/DNA2 velocity ~2-fold

(BTRR/DNA2: 9 ± 6 bp s^{-1}, n=94 molecules; MRN/BLM/DNA2: 9 ± 7 bp s^{-1}, n=30) and decreased processivity by 1.4-fold (BTRR/DNA2: 13 ± 5 kb; MRN/BLM/DNA2: 12 ± 5 kb) (**Figure 1C-E and Supplementary Table 1**). Our results with the human resectosome are consistent with the stimulation of *S. cerevisiae* Sgs1-Dna2 by MRX and Top3-Rmi1 (19, 20). In contrast, the addition of MRN and TOP3A-RMI1/2 to BLM/EXO1 resectosomes did not change the processivity or velocity (~13 $\pm$ 7 kb; ~13 $\pm$ 9 bp s^{-1}; n>50 for all conditions), suggesting that MRN and TOP3A-RMI1/2 selectively regulate DNA2-mediated resection (**Figure 1F,G and Supplementary Table 1**).
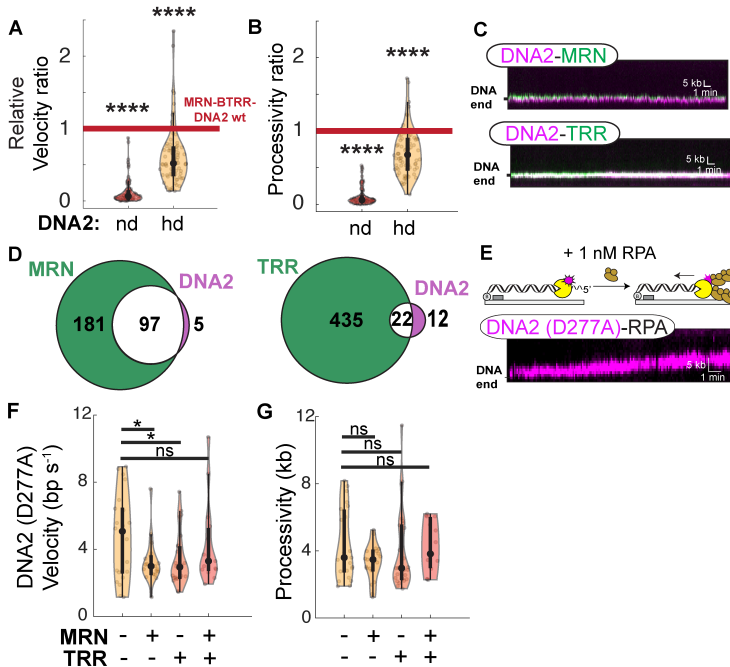
MRN and TOP3A-RMI1/2 recruit DNA2 to free DNA ends
In addition to its nucleolytic activity, DNA2 also encodes a 5'→3' helicase domain that can unwind kilobases of dsDNA (52–56). We first tested the importance of both DNA2's nuclease and helicase activity in DNA resection with MRN and the BTRR complex on the 3'-overhang DNA substrate. As expected, the nuclease-deficient DNA2(D277A) inhibited DNA resection (processivity: 2 ± 2 kb; velocity: 2 ± 2 bp s^{-1}, n=89) (**Figure 2A,B**). Furthermore, a helicase-deficient DNA2(K654R) mutant decreased resection processivity and velocity (processivity: 13 ± 6 kb; velocity: 11 ± 7 bp s^{-1}, n=76). Omitting TOP3A-RMI1/2 and MRN abrogated the negative effects of DNA2(K654R) on resection processivity and velocity (14 ± 8 kb; 12 ± 8 bp s^{-1}, n=42) (**Figure S2A,B**). These results show that both DNA2's nuclease and helicase activity are required for rapid long-range DNA processing.

Since TOP3A-RMI1/2 and MRN stimulate the BLM/DNA2 resectosome, we tested whether either TOP3A-RMI1/2 and/or MRN can stimulate DNA2 alone. MRN recruits DNA2 to DSBs in human cells but does not affect DNA2 nuclease activity *in vitro* (30). Consistent with this report, 95% of DNA2 molecules co-localized with MRN (n=97/102) at free DNA ends (**Figure 2C, D**). We saw a more modest 65% of TOP3A-RMI1/2 complexes (n=22/34) co-localizing with DNA2. DNA2 did not translocate beyond our spatial resolution of ~500 bp with MRN and TOP3A-RMI1/2 (together or independently) in the presence of RPA. Previous studies showed that suppression of DNA2's nuclease activity stimulates processive helicase activity on DNA substrates containing a 5'-flap in the presence of RPA (52–54). To observe the helicase activity, we monitored nuclease-deficient DNA2(D277A) on DNA substrates containing 12 nt 5'-overhang in the presence of 1 nM RPA, similar to previous studies (52, 54, 57). DNA2 was a processive helicase, motoring ~4 ± 2 kb with a velocity of 5 ± 3 bp s^{-1} (n=23 molecules) (**Figure 2E-G and Supplementary Table 2**). The addition of MRN, TOP3A-RMI1/2, or both together had no effect on DNA2's processivity. However, adding either MRN or TOP3A-RMI1/2 decreased DNA2's velocity by ~1.4-fold relative to DNA2(D277A) alone. In contrast, the addition of both MRN and TOP3A-RMI1/2 restored helicase activity to that of DNA2 alone. These results are broadly consistent with a model where MRN and TOP3A-RMI1/2 help DNA2 engage free DNA ends but do not stimulate its nuclease or motor activities.

TOP3A-RMI1/2 helps BLM initiate DNA unwinding
Next, we investigated how TOP3A-RMI1/2 regulates BLM helicase. BLM was fluorescently labeled via a fluorescent anti-HA antibody directed to an N-terminal HA epitope, as we described previously (50). TOP3A-RMI1/2 co-localized with BLM at the free DNA ends (**Figure 3A**). We recently showed that RPA aids BLM in initiating helicase activity from 3'-ssDNA overhangs (50). When RPA is omitted, only ~30% of BLM molecules initiate translocation. However, adding TOP3A-RMI1/2 increases the number of translocating BLM molecules ~2.3-fold (77%; n=86/111) (**Figure 3B**). TOP3A was sufficient to recapitulate most of this stimulation (62%; n=83/133), whereas adding

Figure 2: MRN and TOP3A-RMI1/2 recruits DNA2 to free DNA ends. (A) Ratio of MRN/BTRR/DNA2 velocities and (B) processivities with nuclease-deficient (nd) or helicase-deficient (hd) DNA2 mutants. Both velocity and processivity are compared to the ratios of MRN/BTRR/DNA2 wild-type complex from Figure 1D-E. (ns, p > 0.05; *p < 0.05; **p < 0.01; ***p < 0.001; ****p < 0.0001). (C) Representative kymographs of co-localization of DNA2 (magenta) with MRN and TOP3A-RMI1/2 (TRR; green) at DNA ends. MRN and TRR were imaged in different experiments to guarantee an unambiguous fluorescent signal. (D) Venn diagram that shows MRN and TOP3A-RMI1/2 co-localize DNA2 at free DNA ends. This interaction greatly increases the number of DNA-bound DNA2 molecules. (E) Representative kymograph showing helicase activity of nuclease deficient DNA2 (D277A) mutant in the presence of RPA. (F) Velocities and (G) processivities of DNA2 (D277A) helicase activity with and without TOP3A-RMI1/2 or MRN complex. (not significant; ns, p>0.05; * , p<0.05; **, p<0.01; ***, p<0.001; ****, p<0.0001).

RMI1/2 alone slightly decreased the number of translocating BLM molecules (19%; n=34/182). Finally, adding RPA did not further stimulate the number of translocating BTRR complexes (83%; n=67/81). Surprisingly, although TOP3A-RMI1/2 initiated more BLM helicases, it also decreased BLM's velocity ~2-fold (14 ± 11 bp s^{-1}; n=86) and slightly reduced processivity ~1.2-fold (14 ± 8 kb) (**Figure 3C-D and Supplementary Table 3**). Furthermore, >50% of BTRR molecules dissociate from DNA during the 30-minute experiment (**Figure 4C**). BLM-TOP3A had a similar velocity and processivity as the BTRR complex (n=83). However, the processivity of BLM-RMI1/2 was further reduced ~2-fold compared to the BTRR complex (8 ± 3 kb; n=34). Adding RPA did not change BTRR velocity but slightly decreased the average processivity (11 ± 6 kb; n=67). We conclude that TOP3A-RMI1/2 helps to initiate DNA unwinding but reduces BLM's velocity and processivity.

MRN prevents BTRR dissociation from DNA
Having established that TOP3A-RMI1/2 helps initiate DNA unwinding, we tested whether MRN further stimulates the BTRR complex. MRN is important for BLM recruitment to DSB and has been shown to stimulate

unwinding activity (30, 58, 59). As expected, MRN co-localizes with BTRR and moves together with BTRR during DNA unwinding (**Figure 4A**). In the presence of 1 nM RPA, ~90% (n=131/145) of MRN/BTRR resectosomes initiated DNA unwinding (**Figure 4B**). MRN also retained BLM molecules on the DNA (**Figure 4C**). In the presence of MRN, fewer than 30% of the BLM molecules dissociated from the DNA (n=131). This resulted in a 1.3-fold increase in processivity (15 ± 7 kb; n=131) but a ~1.4-fold decrease in MRN/BTRR helicase velocity (12 ± 8 bp s^{-1}; n=131) (**Figure 4D,E**). We conclude that MRN prevents the dissociation of the BTRR complex from DNA.

MRN synchronizes the BLM and DNA2 motors
DNA2's unwinding rate is ~3-fold slower than BLM's in the presence of RPA (**Figure 2F**). The yeast homolog of BLM, Sgs1, and Dna2 also show a ~2-fold difference in unwinding rates (60). This difference in unwinding rates of BLM and DNA2 can lead to discoordination between the two motors. Consistent with this notion, we observed that ~45% of the BTRR/DNA2 resectosomes paused for >30 seconds during DNA resection (n=42/94) with 12% (n=5/42) of these complexes pausing two or more times during their resection trajectories (**Figure 4G,H**). The change in resection velocity after the pause was heterogeneous and did not correlate with the pre-pause velocity (**Figure S2C**). Adding MRN suppressed these pauses (83% of resectosomes did not pause; n=68/82). MRN also suppresses pauses with the minimal MRN/BLM/DNA2 assembly (83% did not pause; n=25/30). We conclude that MRN coordinates BLM and DNA2 to stimulate efficient DNA resection.
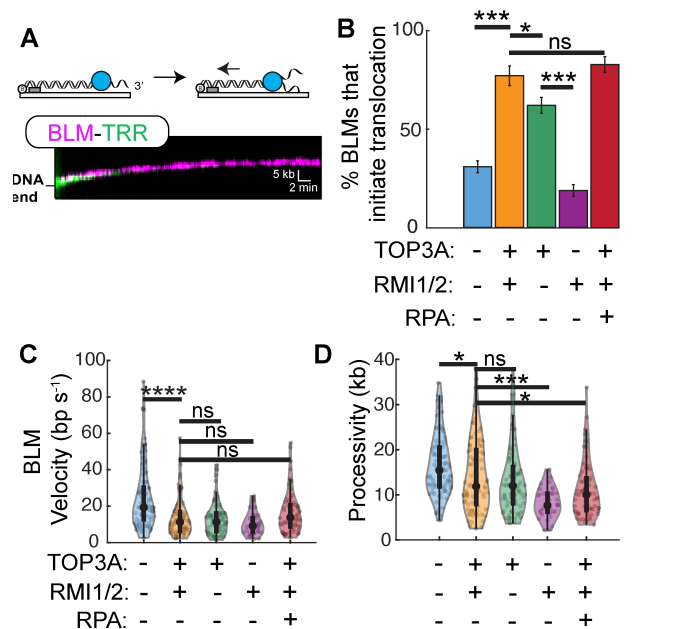
Figure 3. TOP3A-RMI1/2 complex promotes initiation of BLM helicase activity. (A) Representative kymographs showing helicase activity of BLM (magenta) with the TOP3A-RMI1/2 complex (green) along DNA. (B) TOP3A-RMI1/2 stimulates BLM helicase initiation. Error bars: S.D. as determined by bootstrap analysis. (C) Velocities and (D) processivities of the helicase activity of the BTRR complex. (not significant; ns, p>0.05; * , p<0.05; **, p<0.01; ***, p<0.001; ****, p<0.0001).

Soniat al., 2022 – preprint copy - BioRxiv
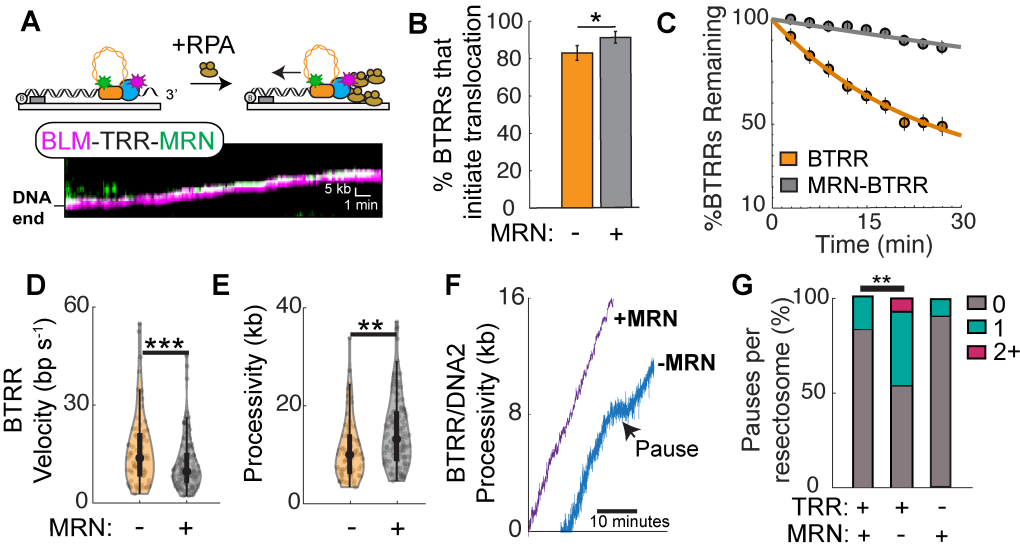
Figure 4: MRN prevents BTRR DNA dissociation. (A) Representative kymographs showing helicase activity of BLM (magenta) with the TOP3A-RMI1/2 complex (dark) and MRN (green) along DNA. (B) MRN has no additional effect on helicase initiation by the BTRR complex with RPA. Error bars: S.D. as determined by bootstrap analysis. (C) MRN retains the BTRR complex on DNA, as indicated by the lifetime analysis of the MRN-BTRR complex. In the presence of MRN, BTRR essentially doesn't dissociate from the DNA during the 30 min experiment. (D) Velocities and (E) processivities of the BTRR complex helicase activity with or without MRN (F) Representative particle tracking of BTRR/DNA2 resection with (purple) and without MRN (blue). (G) MRN decreases pausing events during BTRR/DNA2 resection. (not significant; ns, p>0.05; * , p<0.05; **, p<0.01; ***, p<0.001; ****, p<0.0001).

Discussion

DNA resection is catalyzed by either the EXO1 or DNA2 nucleases. Although EXO1 may be the predominant resection nuclease in human cells (48, 61–63), DNA2 is better at processing apurinic/apyrimidinic (AP) sites and 8-oxo-guanines (64). Furthermore, a super-resolution imaging study found comparable recruitment of both DNA2 and EXO1 at induced DSBs, suggesting that both nucleases are required during DNA resection (59). We had previously shown that MRN and BLM act as processivity factors for EXO1 in the presence of RPA (28, 50). We expand on the earlier study to show that TOP3A-RMI1/2 does not stimulate BLM/EXO1 resection. Instead, TOP3A-RMI1/2, in combination with MRN, stimulate DNA2-mediated resection. Additionally, MRN plays a scaffolding role by assembling the resectosome at a DSB and suppressing the dissociation of BTRR from DNA. MRN also prevents pausing by coordinating BLM and DNA2 during DNA resection **(Figure 5)**.

Pausing during DNA resection has been observed with the bacterial RecBCD nuclease/helicase complex following recognition of the recombination hotspot sequence χ (crossover hotspot instigator-Chi) (65–67). RecBCD is functionally reminiscent of BTRR/DNA2 because it also encodes a fast (RecD) and slow (RecB) motor of opposite polarity. Two motors that move along opposite DNA strands with different speeds will generate a long ssDNA loop between them. Such loops are generated by the *E. coli* RecBCD helicase/nuclease due to differences in the translocation rates between the RecD and RecB motors (68). The molecular origin of RecBCD pausing stems from the slower motor "catching up" with the faster motor due to a conformational switch after χ recognition.

The underlying reason for pausing by BTRR/DNA2 is unknown, but it is unlikely to depend on a χ-like DNA sequence as sequence-dependent resection regulation has not been observed in yeast and human resectosomes. We conjecture that BTRR may unwind DNA in front of DNA2, leading to a growing ssDNA loop that ultimately pauses the entire complex. In this model, MRN prevents the accumulation of such ssDNA loops by synchronizing BLM and DNA2 helicase velocities. In support of this hypothesis, a recent single-molecule study showed that BLM retains contact with ssDNA as it unwinds double-stranded DNA (69). Additional high-resolution electron microscopy and other biochemical studies will be required to directly image an ssDNA loop between BLM and DNA2.

MRE11 and BLM co-localize early at DNA breaks immediately following damage in cells (59). This is consistent with our results showing that MRN assembles the resectosome at a DNA break. However, MRE11 and BLM do not associate as closely in the later stages of DNA resection (59). MRN's role may thus be critical in the initiation and early coordination of BLM and DNA2. In the later stages of DNA resection, pausing may act as a negative DNA resection signal. Such pauses slow resection, possibly limiting over-resection and giving RAD51 sufficient time to complete the homology search. Together, this work shows that its conserved accessory factors regulate BLM's helicase activity and that coordination with MRN and DNA2 stimulates DNA resection and, ultimately, efficient HR.

Materials and Methods

Protein Cloning and Purification

Oligonucleotides were purchased from IDT. Human RPA (pIF47) was purified from *E. coli* using a pET expression vector (48, 70, 71). Epitope-tagged human Exonuclease 1 (EXO1; pIF7) and MRN (pIF926) were purified from insect cells as previously described (28, 48, 50, 72, 73). FLAG-tagged human DNA2 nuclease-deficient (D277A) and helicase-deficient (K654R) mutants were generated by Phusion site-directed mutagenesis (Thermo Fisher) of wild-type DNA2-FLAG (pIF494) using oligos MS0015 and MS0016 for D277A (pIF495) and MS0017 and MS0018 for K564R (pIF496) (**Supplementary Table 4**). Wild-type DNA2, DNA2 (D277A), and DNA2 (K654R) were purified from insect cells as previously described (50, 73).

For single-molecule fluorescent imaging, 3xHA-BLM-His$_6$ (pIF527) was expressed in Sf21 insect cells infected using the Bac-to-
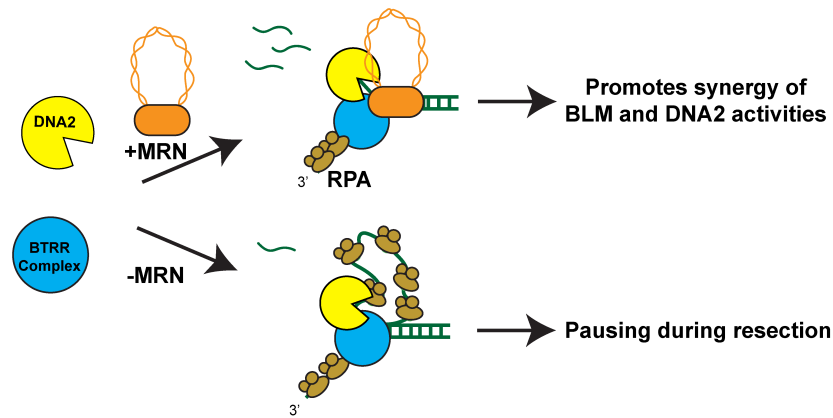
Figure 5: Model of MRN regulation of DNA resection motors

Bac expression system (Life Tech) (74). Cells were harvested 72 hours after infection, pelleted, frozen, and stored at -80°C. Cells were homogenized in buffer A containing 50 mM Tris-HCl pH 7.5, 500 mM NaCl, 10% glycerol, 2 mM β-mercaptoethanol, 10 mM imidazole, and 250 mM phenylmethane sulfonyl fluoride (PMSF) in a Dounce homogenizer (Kimble Chase; Kontes) followed by sonication on ice. Insoluble material was pelleted for 1 hr at 100,000 x g and the supernatant was added to Ni-NTA resin (QIAGEN, 30410) in batch and was eluted with an imidazole gradient containing 50 mM Tris-HCl pH 7.5, 500 mM NaCl, 10% glycerol, 2 mM β-mercaptoethanol, and 10-250 mM Imidazole. BLM fractions were then loaded on a 1 mL HiTrap Heparin (GE Healthcare) and eluted with a gradient from buffer B (50 mM Tris-HCl pH 7.5, 100 mM NaCl, 10% Glycerol, 1 mM DTT) to buffer C (50 mM Tris-HCl pH 7.5, 1 M NaCl, 10% Glycerol, 1 mM DTT). BLM was further purified using a Superose 6 (GE Healthcare) in buffer D (50 mM Tris-HCl pH 7.5, 200 mM NaCl, 10% Glycerol, 1 mM DTT).

pRSF-Duet plasmids containing His_6-TOP3A and RMI1-His_6/FLAG-RMI2 were kindly provided by Patrick Sung and Jim Daley. The TOP3A plasmid was transformed into Rosetta (DE3) pLysS cells and grown in LB media and induced with 0.2 mM IPTG for 18 hours at 16°C. Cells were pelleted and resuspended in buffer E (50 mM Tris-HCl pH 7.5, 1M KCl, 10% glycerol, and 1mM DTT) supplemented with 0.01% Igepal and 1mM PMSF. The cells were sonicated and the soluble material was clarified by centrifugation at 35,000 RCF for 45 minutes. The supernatant was added to Ni-NTA (QIAGEN, 30410) in batch, washed with buffer A supplemented with 20 mM imidazole, and eluted with buffer F (50 mM Tris-HCl pH 7.5, 200 mM KCl, 10% glycerol, 1mM DTT) supplemented with 250mM imidazole. TOP3A was further purified using a 1 mL HiTrap SP (GE Healthcare) with a gradient from buffer G (50 mM Tris-HCl pH 7.5, 50 mM KCl, 10% glycerol, 1mM DTT) to buffer H (50 mM Tris-HCl pH 7.5, 1 M KCl, 10% glycerol, 1mM DTT) and dialyzed overnight at 4°C in buffer I (50 mM Tris-HCl pH 7.5, 200 mM KCl, 10% glycerol, 1mM DTT).

The RMI1-His_6/FLAG-RMI2 plasmid was transformed into Rosetta (DE3) pLysS cells and grown in LB media and induced with 0.2 mM IPTG for 18 hours at 16°C. The cells were sonicated, centrifuged, and purified by Ni-NTA resin similar to TOP3A. RMI1/2 elution from Ni-NTA purification were diluted to 50mM KCl with buffer J (50 mM Tris-HCl pH 7.5, 10% glycerol, 1 mM DTT), loaded on a 5mL HiTrap Q XL (GE Healthcare), and eluted with a gradient with buffers G and H. RMI1/2 was further purified using a Superdex 200 Increase (GE Healthcare) in buffer I. The TOP3A-RMI1/2 complex was assembled by incubating purified TOP3A and RMI1/2 (1:3 ratio) followed by purification using a Superdex 200 Increase (GE Healthcare) in buffer I.

Single-Molecule Fluorescence Microscopy
All single-molecule data were collected on a Nikon Ti-E microscope in a prism-TIRF configuration equipped with a Prior H117 motorized stage. Flowcells were loaded into a custom-designed stage insert incorporating a chip mount, fluidic interface, and heating element (49). All experiments were maintained at 37°C by a combination of an objective heater (Bioptechs) and a custom-built stage-mounted heating block. The flowcell was illuminated with a 488 nm laser (Coherent) through a quartz prism (Tower Optical Co.). Data were collected with a 200 ms exposure, 2-second shutter (Vincent Associates) resulting in 1,800 frames in 1 hour, through a 60X water-immersion objective (1.2NA, Nikon), a 500 nm long-pass (Chroma), and a 638 nm dichroic beam splitter (Chroma), which allowed two-channel detection through two EMCCD cameras (Andor iXon DU897, cooled to -80°C). Images were collected using NIS-Elements software and saved in an uncompressed TIFF file format for later analysis (see below).

Fluorescent particles were tracked in ImageJ using a custom-written particle tracking script (available upon request). The resulting trajectories were analyzed in Matlab (Mathworks). Trajectories were used to calculate velocity and processivity for resectosomes. DNA substrates for single-molecule studies contained a 78 nt 3'-overhang or 12 nt 5'-overhang. These were prepared by annealing oligonucleotides IF007 and LM003 (3'-overhang) or IF007 only (5'-overhang) (**Supplementary Table 4**) (28).

Fluorescent protein labeling
3xHA-BLM (40 nM) were conjugated to Quantum Dots (QDs) pre-incubated with a rabbit anti-HA antibody (ICL Lab) on ice for 10 minutes in 20 μL. Next, BLM was incubated with the anti-HA QDs at a ratio of 1:2 for an additional 10 minutes on ice, diluted with imaging buffer (40 mM Tris pH 8.0, 60 mM NaCl, 200 μg/mL BSA, 2 mM DTT, 2 mM $MgCl_2$, 1 mM ATP) to 200 μL and injected into the flowcell. FLAG-TOP3A-RMI1/2 or FLAG-DNA2 were labeled with QDs pre-incubated with a mouse anti-FLAG antibody (Sigma-Aldrich) on ice for 10 minutes prior to injection. Additionally, biotin-MRN was labeled via streptavidin QDs. Saturating biotin was added to the protein-QD conjugates to bind free streptavidin sites prior to injection

Quantification and Statistical Analysis
For Figures 1-4, n represents the number of molecules. Quantification and statistical analyses were done using MATLAB (version: R2015b). Fluorescent particles were tracked using an in-house ImageJ script (available upon request) where the positions of individual molecules on DNA were determined by fitting the point spread function to a 2D Gaussian. Trajectories were used to calculate the velocity and

processing for BLM and DNA resection complexes. Statistical details of experiments can be found in the Results and figure legends where indicated.

References

1. Jasin, M., and Rothstein, R. (2013) Repair of strand breaks by homologous recombination. *Cold Spring Harb Perspect Biol*. **5**, a012740

2. Mathiasen, D. P., and Lisby, M. (2014) Cell cycle regulation of homologous recombination in Saccharomyces cerevisiae. *FEMS Microbiol. Rev.* **38**, 172–184

3. Cejka, P. (2015) DNA End Resection: Nucleases Team Up with the Right Partners to Initiate Homologous Recombination. *J. Biol. Chem.* **290**, 22931–22938

4. Heyer, W.-D., Ehmsen, K. T., and Liu, J. (2010) Regulation of Homologous Recombination in Eukaryotes. *Annu. Rev. Genet.* **44**, 113–139

5. Huertas, P. (2010) DNA resection in eukaryotes: deciding how to fix the break. *Nat Struct Mol Biol*. **17**, 11–16

6. Mimitou, E. P., and Symington, L. S. (2008) Sae2, Exo1 and Sgs1 collaborate in DNA double-strand break processing. *Nature*. **455**, 770–774

7. Myler, L. R., and Finkelstein, I. J. (2017) Eukaryotic resectosomes: A single-molecule perspective. *Progress in Biophysics and Molecular Biology*. **127**, 119–129

8. Ronato, D. A., Mersaoui, S. Y., Busatto, F. F., Affar, E. B., Richard, S., and Masson, J.-Y. (2020) Limiting the DNA Double-Strand Break Resectosome for Genome Protection. *Trends in Biochemical Sciences*. **45**, 779–793

9. San Filippo, J., Sung, P., and Klein, H. (2008) Mechanism of Eukaryotic Homologous Recombination. *Annu. Rev. Biochem.* **77**, 229–257

10. Symington, L. S. (2016) Mechanism and regulation of DNA end resection in eukaryotes. *Crit. Rev. Biochem. Mol. Biol.* **51**, 195–212

11. Symington, L. S., and Gautier, J. (2011) Double-strand break end resection and repair pathway choice. *Annual review of genetics*. **45**, 247–71

12. Zhao, F., Kim, W., Kloeber, J. A., and Lou, Z. (2020) DNA end resection and its role in DNA replication and DSB repair choice in mammalian cells. *Exp Mol Med*. **52**, 1705–1714

13. Lisby, M., Barlow, J. H., Burgess, R. C., and Rothstein, R. (2004) Choreography of the DNA Damage Response: Spatiotemporal Relationships among Checkpoint and Repair Proteins. *Cell*. **118**, 699–713

14. Bell, J. C., and Kowalczykowski, S. C. (2016) Mechanics and Single-Molecule Interrogation of DNA Recombination. *Annu. Rev. Biochem.* 10.1146/annurev-biochem-060614-034352

15. Chen, R., and Wold, M. S. (2014) Replication Protein A: Single-stranded DNA's first responder : Dynamic DNA-interactions allow Replication Protein A to direct single-strand DNA intermediates into different pathways for synthesis or repair. *Bioessays*. **36**, 1156–1161

16. Kowalczykowski, S. C. (2015) An Overview of the Molecular Mechanisms of Recombinational DNA Repair. *Cold Spring Harb Perspect Biol*. 10.1101/cshperspect.a016410

17. Morrical, S. W. (2015) DNA-Pairing and Annealing Processes in Homologous Recombination and Homology-Directed Repair. *Cold Spring Harb Perspect Biol*. **7**, a016444

18. Cejka, P., and Symington, L. S. (2021) DNA End Resection: Mechanism and Control. *Annu. Rev. Genet.* **55**, 285–307

19. Cejka, P., Cannavo, E., Polaczek, P., Masuda-Sasa, T., Pokharel, S., Campbell, J. L., and Kowalczykowski, S. C. (2010) DNA end resection by Dna2-Sgs1-RPA and its stimulation by Top3-Rmi1 and Mre11-Rad50-Xrs2. *Nature*. **467**, 112–116

20. Niu, H., Chung, W.-H., Zhu, Z., Kwon, Y., Zhao, W., Chi, P., Prakash, R., Seong, C., Liu, D., Lu, L., Ira, G., and Sung, P. (2010) Mechanism of the ATP-dependent DNA end-resection machinery from Saccharomyces cerevisiae. *Nature*. **467**, 108–111

21. Cannavo, E., and Cejka, P. (2014) Sae2 promotes dsDNA endonuclease activity within Mre11-Rad50-Xrs2 to resect DNA breaks. *Nature*. **514**, 122–125

22. Chanut, P., Britton, S., Coates, J., Jackson, S. P., and Calsou, P. (2016) Coordinated nuclease activities counteract Ku at single-ended DNA double-strand breaks. *Nat Commun*. **7**, 12889

23. Garcia, V., Phelps, S. E., Gray, S., and Neale, M. J. (2011) Bidirectional resection of DNA double-strand breaks by Mre11 and Exo1. *Nature*. **479**, 241–4

24. Neale, M. J., Pan, J., and Keeney, S. (2005) Endonucleolytic processing of covalent protein-linked DNA double-strand breaks. *Nature*. **436**, 1053–1057

25. Paull, T. T., and Gellert, M. (1998) The 3′ to 5′ Exonuclease Activity of Mre11 Facilitates Repair of DNA Double-Strand Breaks. *Molecular Cell*. **1**, 969–979

26. Shibata, A., Moiani, D., Arvai, A. S., Perry, J., Harding, S. M., Genois, M.-M., Maity, R., van Rossum-Fikkert, S., Kertokalio, A., Romoli, F., Ismail, A., Ismalaj, E., Petricci, E., Neale, M. J., Bristow, R. G., Masson, J.-Y., Wyman, C., Jeggo, P. A., and Tainer, J. A. (2014) DNA double-strand break repair pathway choice is directed by distinct MRE11 nuclease activities. *Mol. Cell*. **53**, 7–18

27. Llorente, B., and Symington, L. S. (2004) The Mre11 Nuclease Is Not Required for 5′ to 3′ Resection at Multiple HO-Induced Double-Strand Breaks. *Mol Cell Biol*. **24**, 9682–9694

28. Myler, L. R., Gallardo, I. F., Soniat, M. M., Deshpande, R. A., Gonzalez, X. B., Kim, Y., Paull, T. T., and Finkelstein, I. J. (2017)

Single-Molecule Imaging Reveals How Mre11-Rad50-Nbs1 Initiates DNA Break Repair. *Molecular Cell*. **67**, 891-898.e4

29. Nicolette, M. L., Lee, K., Guo, Z., Rani, M., Chow, J. M., Lee, S. E., and Paull, T. T. (2010) Mre11-Rad50-Xrs2 and Sae2 promote 5' strand resection of DNA double-strand breaks. *Nat. Struct. Mol. Biol.* **17**, 1478–1485

30. Nimonkar, A. V., Genschel, J., Kinoshita, E., Polaczek, P., Campbell, J. L., Wyman, C., Modrich, P., and Kowalczykowski, S. C. (2011) BLM-DNA2-RPA-MRN and EXO1-BLM-RPA-MRN constitute two DNA end resection machineries for human DNA break repair. *Genes Dev.* **25**, 350–362

31. Shim, E. Y., Chung, W. H., Nicolette, M. L., Zhang, Y., Davis, M., Zhu, Z., Paull, T. T., Ira, G., and Lee, S. E. (2010) Saccharomyces cerevisiae Mre11/Rad50/Xrs2 and Ku proteins regulate association of Exo1 and Dna2 with DNA breaks. *The EMBO journal*. **29**, 3370–80

32. Zhu, Z., Chung, W.-H., Shim, E. Y., Lee, S. E., and Ira, G. (2008) Sgs1 helicase and two nucleases Dna2 and Exo1 resect DNA double-strand break ends. *Cell*. **134**, 981–994

33. Bythell-Douglas, R., and Deans, A. J. (2021) A Structural Guide to the Bloom Syndrome Complex. *Structure*. **29**, 99–113

34. Hodson, C., Low, J. K. K., van Twest, S., Jones, S. E., Swuec, P., Murphy, V., Tsukada, K., Fawkes, M., Bythell-Douglas, R., Davies, A., Holien, J. K., O'Rourke, J. J., Parker, B. L., Glaser, A., Parker, M. W., Mackay, J. P., Blackford, A. N., Costa, A., and Deans, A. J. (2022) Mechanism of Bloom syndrome complex assembly required for double Holliday junction dissolution and genome stability. *Proc. Natl. Acad. Sci. U.S.A.* **119**, e2109093119

35. Manthei, K. A., and Keck, J. L. (2013) The BLM dissolvasome in DNA replication and repair. *Cell. Mol. Life Sci.* **70**, 4067–4084

36. Singh, T. R., Ali, A. M., Busygina, V., Raynard, S., Fan, Q., Du, C.-h., Andreassen, P. R., Sung, P., and Meetei, A. R. (2008) BLAP18/RMI2, a novel OB-fold-containing protein, is an essential component of the Bloom helicase-double Holliday junction dissolvasome. *Genes & Development*. **22**, 2856–2868

37. Wu, L., and Hickson, I. D. The Bloom's syndrome helicase stimulates the activity of human topoisomerase IIIa

38. Xu, D., Guo, R., Sobeck, A., Bachrati, C. Z., Yang, J., Enomoto, T., Brown, G. W., Hoatlin, M. E., Hickson, I. D., and Wang, W. (2008) RMI, a new OB-fold complex essential for Bloom syndrome protein to maintain genome stability. *Genes & Development*. **22**, 2843–2855

39. Yin, J., Sobeck, A., Xu, C., Meetei, A. R., Hoatlin, M., Li, L., and Wang, W. (2005) BLAP75, an essential component of Bloom's syndrome protein complexes that maintain genome integrity. *EMBO J.* **24**, 1465–1476

40. Chan, K.-L., North, P. S., and Hickson, I. D. (2007) BLM is required for faithful chromosome segregation and its localization defines a class of ultrafine anaphase bridges. *EMBO J.* **26**, 3397–3409

41. Croteau, D. L., Popuri, V., Opresko, P. L., and Bohr, V. A. (2014) Human RecQ helicases in DNA repair, recombination, and replication. *Annu. Rev. Biochem.* **83**, 519–552

42. Davies, S. L., North, P. S., and Hickson, I. D. (2007) Role for BLM in replication-fork restart and suppression of origin firing after replicative stress. *Nature Structural & Molecular Biology*. **14**, 677–679

43. Shorrocks, A.-M. K., Jones, S. E., Tsukada, K., Morrow, C. A., Belblidia, Z., Shen, J., Vendrell, I., Fischer, R., Kessler, B. M., and Blackford, A. N. (2021) The Bloom syndrome complex senses RPA-coated single-stranded DNA to restart stalled replication forks. *Nat Commun*. **12**, 585

44. Daley, J. M., Chiba, T., Xue, X., Niu, H., and Sung, P. (2014) Multifaceted role of the Topo IIIα-RMI1-RMI2 complex and DNA2

45. Sturzenegger, A., Burdova, K., Kanagaraj, R., Levikova, M., Pinto, C., Cejka, P., and Janscak, P. (2014) DNA2 cooperates with the WRN and BLM RecQ helicases to mediate long-range DNA end resection in human cells. *J. Biol. Chem.* **289**, 27314–27326

46. Bizard, A. H., and Hickson, I. D. (2014) The dissolution of double Holliday junctions. *Cold Spring Harb Perspect Biol*. **6**, a016477

47. Wu, L., and Hickson, I. D. (2003) The Bloom's syndrome helicase suppresses crossing over during homologous recombination. *Nature*. **426**, 870–874

48. Myler, L. R., Gallardo, I. F., Zhou, Y., Gong, F., Yang, S.-H., Wold, M. S., Miller, K. M., Paull, T. T., and Finkelstein, I. J. (2016) Single-molecule imaging reveals the mechanism of Exo1 regulation by single-stranded DNA binding proteins. *Proc. Natl. Acad. Sci. U.S.A.* **113**, e1170–e1179

49. Soniat, M. M., Myler, L. R., Schaub, J. M., Kim, Y., Gallardo, I. F., and Finkelstein, I. J. (2017) Next-Generation DNA Curtains for Single-Molecule Studies of Homologous Recombination. *Meth. Enzymol.* **592**, 259–281

50. Soniat, M. M., Myler, L. R., Kuo, H.-C., Paull, T. T., and Finkelstein, I. J. (2019) RPA Phosphorylation Inhibits DNA Resection. *Molecular Cell*. **75**, 145-153.e5

51. Gallardo, I. F., Pasupathy, P., Brown, M., Manhart, C. M., Neikirk, D. P., Alani, E., and Finkelstein, I. J. (2015) High-Throughput Universal DNA Curtain Arrays for Single-Molecule Fluorescence Imaging. *Langmuir*. **31**, 10310–10317

52. Levikova, M., Klaue, D., Seidel, R., and Cejka, P. (2013) Nuclease activity of Saccharomyces cerevisiae Dna2 inhibits its potent DNA helicase activity. *Proc. Natl. Acad. Sci. U.S.A.* **110**, E1992-2001

53. Levikova, M., Pinto, C., and Cejka, P. (2017) The motor activity of DNA2 functions as an ssDNA translocase to promote DNA end resection. *Genes Dev.* **31**, 493–502

54. Pinto, C., Kasaciunaite, K., Seidel, R., and Cejka, P. (2016) Human DNA2 possesses a cryptic DNA unwinding activity that functionally integrates with BLM or WRN helicases. *Elife*. 10.7554/eLife.18574

55. Shen, J., Zhao, Y., Pham, N. T., Li, Y., Zhang, Y., Trinidad, J., Ira, G., Qi, Z., and Niu, H. (2022) Deciphering the mechanism of processive ssDNA digestion by the Dna2-RPA ensemble. *Nat Commun*. **13**, 359

56. Zheng, L., Meng, Y., Campbell, J. L., and Shen, B. (2020) Multiple roles of DNA2 nuclease/helicase in DNA metabolism, genome stability and human diseases. *Nucleic Acids Research*. **48**, 16–35

57. Ceppi, I., Howard, S. M., Kasaciunaite, K., Pinto, C., Anand, R., Seidel, R., and Cejka, P. (2020) CtIP promotes the motor activity of DNA2 to accelerate long-range DNA end resection. *Proc Natl Acad Sci USA*. **117**, 8859–8869

58. Tripathi, V., Agarwal, H., Priya, S., Batra, H., Modi, P., Pandey, M., Saha, D., Raghavan, S. C., and Sengupta, S. (2018) MRN complex-dependent recruitment of ubiquitylated BLM helicase to DSBs negatively regulates DNA repair pathways. *Nat Commun*. **9**, 1016

59. Whelan, D. R., and Rothenberg, E. (2021) Super-resolution mapping of cellular double-strand break resection complexes during homologous recombination. *Proc Natl Acad Sci USA*. **118**, e2021963118

60. Kasaciunaite, K., Fettes, F., Levikova, M., Daldrop, P., Anand, R., Cejka, P., and Seidel, R. (2019) Competing interaction partners modulate the activity of Sgs1 helicase during DNA end resection. *EMBO J.* 10.15252/embj.2019101516

61. Farah, J. A., Cromie, G. A., and Smith, G. R. (2009) Ctp1 and Exonuclease 1, alternative nucleases regulated by the MRN

Soniat al., 2022 – preprint copy - BioRxiv

complex, are required for efficient meiotic recombination. *Proc. Natl. Acad. Sci. U.S.A.* **106**, 9356–9361

62. Tomimatsu, N., Mukherjee, B., Deland, K., Kurimasa, A., Bolderson, E., Khanna, K. K., and Burma, S. (2012) Exo1 plays a major role in DNA end resection in humans and influences double-strand break repair and damage signaling decisions. *DNA Repair (Amst.)*. **11**, 441–448

63. Zhou, Y., Caron, P., Legube, G., and Paull, T. T. (2014) Quantitation of DNA double-strand break resection intermediates in human cells. *Nucleic Acids Res.* **42**, e19

64. Daley, J. M., Tomimatsu, N., Hooks, G., Wang, W., Miller, A. S., Xue, X., Nguyen, K. A., Kaur, H., Williamson, E., Mukherjee, B., Hromas, R., Burma, S., and Sung, P. (2020) Specificity of end resection pathways for double-strand break regions containing ribonucleotides and base lesions. *Nat Commun*. **11**, 3088

65. Liu, B., Baskin, R. J., and Kowalczykowski, S. C. (2013) DNA unwinding heterogeneity by RecBCD results from static molecules able to equilibrate. *Nature*. **500**, 482–485

66. Spies, M., Bianco, P. R., Dillingham, M. S., Handa, N., Baskin, R. J., and Kowalczykowski, S. C. (2003) A molecular throttle: the recombination hotspot chi controls DNA translocation by the RecBCD helicase. *Cell*. **114**, 647–654

67. Spies, M., Amitani, I., Baskin, R. J., and Kowalczykowski, S. C. (2007) RecBCD enzyme switches lead motor subunits in response to chi recognition. *Cell*. **131**, 694–705

68. Taylor, A. F., and Smith, G. R. (2003) RecBCD enzyme is a DNA helicase with fast and slow motors of opposite polarity. *Nature*. **423**, 889–893

69. Xue, C., Salunkhe, S. J., Tomimatsu, N., Kawale, A. S., Kwon, Y., Burma, S., Sung, P., and Greene, E. C. (2022) Bloom helicase mediates formation of large single–stranded DNA loops during DNA end processing. *Nat Commun*. **13**, 2248

70. Binz, S. K., Lao, Y., Lowry, D. F., and Wold, M. S. (2003) The phosphorylation domain of the 32-kDa subunit of replication protein A (RPA) modulates RPA-DNA interactions. Evidence for an intersubunit interaction. *J. Biol. Chem.* **278**, 35584–35591

71. Modesti, M. (2011) Fluorescent Labeling of Proteins. in *Single Molecule Analysis* (Peterman, E. J. G., and Wuite, G. J. L. eds), pp. 101–120, Humana Press, Totowa, NJ, **783**, 101–120

72. Myler, L. R., Soniat, M. M., Zhang, X., Deshpande, R. A., Paull, T. T., and Finkelstein, I. J. (2019) Purification and Biophysical Characterization of the Mre11-Rad50-Nbs1 Complex. *Methods Mol. Biol.* **2004**, 269–287

73. Soniat, M. M., Myler, L. R., and Finkelstein, I. J. (2019) Assembling the Human Resectosome on DNA Curtains. *Methods Mol. Biol.* **1999**, 225–244

74. Yang, S.-H., Zhou, R., Campbell, J., Chen, J., Ha, T., and Paull, T. T. (2013) The SOSS1 single-stranded DNA binding complex promotes DNA end resection in concert with Exo1. *EMBO J.* **32**, 126–139